Formation of Reactive Nitrogen Species Promoted by Iron Ions through the Photochemistry of a Neonicotinoid Insecticide

Zhu Ran[1,2], Yanan Hu[1,2,3*], Yuanzhe Li[1,2], Xiaoya Gao[1,2], Can Ye[4], Shuai Li[5], Xiao Lu[5], Yongming Luo[1,2,3], Sasho Gligorovski [6,7,8*], Jiangping Liu[1,2*]

[1]Faculty of Environmental Science and Engineering, Kunming University of Science and Technology, Kunming 650500, China;
[2]The Innovation Team for Volatile Organic Compounds Pollutants Control and Resource Utilization of Yunnan Province, The Higher Educational Key Laboratory for Odorous Volatile Organic Compounds Pollutants Control of Yunnan Province, Kunming 650500, China;
[3]Faculty of Chemical Engineering, Kunming University of Science and Technology, Kunming 650500, China;
[4]Faculty of Environmental Science and Engineering, Peking University, Beijing 100871, China;
[5]School of Atmospheric Sciences, Sun Yat-sen University, Southern Marine Science and Engineering Guangdong Laboratory (Zhuhai), Zhuhai, Guangdong 519082, China;
[6]State Key Laboratory of Organic Geochemistry and Guangdong Provincial Key Laboratory of Environmental Protection and Resources Utilization, Guangzhou Institute of Geochemistry, Chinese Academy of Sciences, Guangzhou 510640, China
[7]Guangdong-Hong Kong-Macao Joint Laboratory for Environmental Pollution and Control, Guangzhou Institute of Geochemistry, Chinese Academy of Science, Guangzhou 510640, China;
[8]Chinese Academy of Science, Center for Excellence in Deep Earth Science, Guangzhou, 510640, China.

Correspondence to: gligorovski@gig.ac.cn; liujiangping18@mails.ucas.ac.cn; huyanan0917@163.com

Abstract. Nitrous acid (HONO) and nitrogen oxides (NOx = NO + NO_2) are important atmospheric pollutants and key intermediates in the global nitrogen cycle, but their sources and formation mechanisms are still poorly understood. Here, we investigated the effect of soluble iron (Fe^{3+}) on the photochemical behaviour of a widely used neonicotinoid (NN) insecticide, nitenpyram (NPM), in the aqueous phase. The yields of HONO and NOx increased significantly when NPM solution was irradiated in the presence of iron ions (Fe^{3+}). We propose that the enhanced HONO and NO_2 emissions from the photodegradation of NPM in the presence of iron ions result from the redox cycle between Fe^{3+} and Fe^{2+} and the generated reactive oxygen species (ROS) by the electron transfer between the excited triplet state of NPM and the molecular oxygen (O_2). Using the laboratory-derived parametrization based on kinetic data and gridded downward solar radiation, we estimate that the photochemistry of NPM induced by Fe^{3+} releases 0.50 and 0.77 Tg N $year^{-1}$ of NOx and HONO to the atmosphere, respectively.

This study suggests a novel source of HONO and NOx during daytime and potentially helps to narrow the gap between the field observations and model outcomes of HONO in the atmosphere. The suggested photochemistry of NPM can be an important contribution to the global nitrogen cycle affecting the atmospheric oxidizing capacity as well as the climate change.

1 Introduction

Neonicotinoids (NNs) are a class of systemic insecticides that have been widely used in agriculture and horticulture since the 1990s (Bass et al., 2015) accounting for one-third of the total world insecticide market (Simon et al., 2015) with growing use in the past decades (Botías et al., 2015; Morrissey et al., 2015). They are highly water-soluble and persistent in the environment, and can be transported to surface waters via runoff, leaching, or spray drift. NNs have been detected in various aquatic ecosystems, such as rivers, lakes, wetlands, and coastal waters, at concentrations ranging from 12.45 ng L^{-1} to 225 μg L^{-1} (Pan et al., 2020; Anderson et al., 2013). Increasing public perception of NNs insecticides pollution, led to significant research efforts devoted to revealing the effect of insecticide application on human (Cimino et al., 2017; Han et al., 2018), birds (Hallmann et al., 2014; Millot et al., 2017) , animals (Morrissey et al., 2015; Gibbons et al., 2015) and pollinators (especially bees) (Kessler et al., 2015; Raine et al., 2015; Goulson et al., 2015). In the environment, NNs insecticides can undergo various chemical processes, photolysis being one of the major fate (Lu et al., 2015; González-Mariño et al., 2018). Recent studies have focused mainly on photochemistry of NNs insecticides and related atmospheric lifetimes, and quantum yields (Lu et al., 2015; González-Mariño et al., 2018; Aregahegn et al., 2017; Aregahegn et al., 2018). It has been shown that the ozonolysis of NNs insecticides on various surfaces could contribute to the formation of gaseous nitrous acid (HONO) (Wang et al., 2020). Gaseous nitrous oxide (N_2O), which is a potent greenhouse gas, was previously identified as the gas-phase product in the photolysis of solid thin films of NNs (Nitenpyram, acetamiprid, thiamethoxam, thiacloprid, clothianidin and dinotefuran), with yields of $\Delta N_2O/\Delta NN > 0.5$ in air at both 313 and 254 nm (Wang et al., 2019; Aregahegn et al., 2017; Aregahegn et al., 2018). Palma et al (Palma et al., 2020) used a gas-flow reactor connecting with a

NOx analyzer, and the production of gaseous NO/NO_2 was founded during irradiation (300-450 nm) of imidacloprid. However, the crucial role of the NNs insecticides in the global nitrogen cycle at the air-water interface is largely unknown.

Nitenpyram (NPM) is one of the most commonly used NNs insecticides. It represents a systemic NNs insecticide which is widely distributed among soil, dust particles and in the aqueous environment (Botías et al., 2015; Ezell et al., 2019). Once released in the environment, NPM will be transformed into other products by absorbing sunlight (λ>290 nm) and/or reacting with atmospheric oxidants such as the hydroxyl radical (OH) and ozone (O_3) (Wang et al., 2020). The NPM is a nitroalkene, which is structurally similar to nitroaromatic compounds ($Ar\text{-}NO_2$). Previous studies have indicated that the photolysis of $Ar\text{-}NO_2$ can be a source of HONO and NOx in the atmosphere (Fukuhara et al., 2006; Yang et al., 2001; Bejan et al., 2021). HONO represents one of the main sources of OH radicals in the urban atmosphere contributing by up to 80% of the total OH production (Alicke et al., 2003; Young et al., 2012; Zheng et al., 2020). The main identified HONO sources in the urban air are the photolysis of nitrates (Ye et al., 2017; Gen et al., 2021) and light-induced heterogeneous reaction of NO_2 with environmental surfaces (Liu et al., 2019; Liu et al., 2020; Liu et al., 2023; Monge et al., 2010; Han et al., 2016). Yet, there is a discrepancy between the modeled HONO values and field observations of HONO during the daytime, suggesting that there are missing HONO sources in the atmosphere. Meanwhile, the quantification of NOx is also of great significance for the atmospheric cycle of nitrogen species as NOx plays a crucial role in the photochemical smog and acid rain formation. Therefore, it is worthwhile to explore the contribution of NPM photolysis to HONO and NOx, which in turn can offer a guidance for the development of more sustainable next generation insecticide products.

Iron species are ubiquitous on earth surfaces, including water, soil and air-water interface (Gen et al., 2021). Recent study (Kebede et al., 2016) showed that one of less explored HONO sources could be highly dependent on the photochemical reaction of iron. The photosensitivity, oxidation state and catalytic properties of iron could enable it to possibly react with NNs insecticides compounds which are enriched at air-water interface. Previous studies on the mechanism of NNs oxidation in the ferric aqueous phase have focused on the photo-Fenton reaction (Malato et al., 2021; Lacson et al., 2018; Wang et al., 2022; Nguyen et al., 2020; Sedaghat et al., 2016) and heterogeneous-phase photocatalysis (Rózsa et al., 2019; Sun et al., 2019; Hayat., 2019; Soltani-nezhad., 2019). As recently reported, the photolysis of iron can generate several reactive oxygen species (ROS) such as $O_2\bullet^-/HO_2\bullet$, which can trigger the redox cycle between Fe^{3+} and Fe^{2+} (Gen et al., 2021) as well as promote NNs insecticides oxidation. Meanwhile, iron ions inhibit the degradation of organic matter through the formation of complexes, mainly due to fluorescence bursting. The complexation may cause the inhibition of the excited singlet state and thus the photoformation of the triplet excited state (Wan et al., 2019). In addition to the NN insecticides and iron photosensitizers, the nitrate (NO_3^-) and nitrite (NO_2^-) can also absorb sunlight in the actinic region and initiate production of ROS (Vione et al., 2019). Moreover, the reaction between Fe^{2+} and NO_3^- may be a potentially important source of HONO (Gen et al., 2021). To this end, we suggest that the photolysis of NPM in the presence of iron may contribute to a missing atmospheric HONO source.

To our knowledge, this is a first investigation to measure the photochemical production of HONO and NOx from NPM photolysis in absence and in the presence of soluble iron. The photolysis frequency of HONO ($J_{NPM \rightarrow HONO}$), NO_2 ($J_{NPM \rightarrow NO2}$) and NO ($J_{NPM \rightarrow NO}$) during the NPM reaction at the air-water interface was investigated. The kinetics and mechanism of HONO and NOx formation in the presence of soluble iron were evaluated. This study highlights an overlooked source of HONO and NOx from NNs-covered water surfaces which may play a critical role in atmospheric nitrogen cycle and evaluation of the atmospheric oxidation capacity.

2 Experimental

2.1 Materials and Sample Preparation

Solid NPM (Aladdin, China) was dissolved in ultra-pure water to prepare an aqueous NPM solution (0.5 mg mL^{-1}) before each experiment. $FeCl_3$ (98%, Aladdin China) was used as the source of different concentrations of aqueous Fe^{3+} (0.1-0.8 mg mL^{-1}), and their solutions were prepared by dissolving the corresponding mass of $FeCl_3$ in ultra-pure water.

2.2 Experimental Setup

The circular reactor consisted of a double layer of quartz glass (3.4 cm height, 7.5 cm inner diameter) connected to a thermostatic bath (XOSC-20, China), which allowed operation at a constant temperature of 298 K (Figure S1). The previously prepared sample solution was placed in the circular reactor and exposed to a Xenon lamp (Perfect Light, PLS-SXE 300, China) vertically above the reactor. The Xenon lamp was 12 cm away from the liquid level of NPM. The spectral irradiance of the Xenon lamp was measured by a calibrated spectroradiometer (HP 350 UVP, China) (Figure S1). Dry air collected from an air generator (HY-3, China) was used for the experiment. During the whole experiment, a constant flow of 800 mL min^{-1} of dry air was controlled by an electronic soap film flowmeter (SCal Plus, China). The UV absorption spectra of the NPM aqueous solutions in the absence and in the presence of iron ions were measured by the UV-vis double-beam spectrophotometer (Shimadzu 2600, Japan) (Figure S2, Text S1).

2.3 NOx, HONO, NPM and ROS measurements

NO, NO_2 and HONO were detected using a chemiluminescence NOx analyzer (42i, THERMO) with a molybdenum converter. NO was measured by reacting NO with O_3 to produce characteristic luminescence, and the intensity of luminescence was proportional to the concentration of NO. In the detection of NO_2, a molybdenum catalyst was used to convert NO_2 to NO. A quartz tube (25 cm length, 2.9 cm inner diameter) filled with a certain amount of crystalline Na_2CO_3 was introduced to capture HONO between the circular reactor outlet and the NOx analyzer. It is well known that almost all HONO molecules can contact Na_2CO_3 when using molybdenum converters, achieving high capture efficiency of HONO. Therefore, HONO can be indirectly quantified by the difference between the NO_2 signal and the Na_2CO_3 tube (Monge et al., 2010; Cazoir et al., 2014; Brigante et al., 2008; Zhou et al., 2018). The quantification of NPM before and after the reaction

was determined by High performance liquid chromatography (HPLC). The mobile phase was a mixture of water and acetonitrile with a flow rate of 0.5 mL min^{-1} at 80:20 (v/v). The column temperature was kept at 30°C, the injection volume was 20 μL, and the detection wavelength was set to 270 nm. The external standard method was used for the quantitative determination of NPM. Photoproductions of O_2-•, $^1O_2$ and •OH (ROS) were quantified using DMPO, TEMP and DMPO as chemical probe molecules, respectively.

2.4 Kinetic Analysis

The NPM photolysis kinetics was described using a first-order reaction (Eq.(1)), and the half-life ($t_{1/2}$) was calculated using Eq.(2).

$$C_t = C_0 \times e^{-kt} \quad (1)$$

$$t_{1/2} = \ln(2)/k \quad (2)$$

where C_0 (mg ml^{-1}) is initial concentration of NPM, C_t (mg ml^{-1}) is the NPM concentration at time t, and k is the first-order rate constant.

2.5 The photolysis frequency

The photolysis frequencies of NPM to HONO and NOx were calculated by Eq.(3) and Eq.(4), respectively.

$$J_{NPM\rightarrow HONO} = \frac{QM_{NPM}\int_0^t C_t^{HONO}dt}{60\times10^{-3}N_A\times t\times(m_0+m_t)/2} \quad (3)$$

$$J_{NPM\rightarrow NOx} = \frac{QM_{NPM}\int_0^t C_t^{NOx}dt}{60\times10^{-3}N_A\times t\times(m_0+m_t)/2} \quad (4)$$

Where Q (mL min^{-1}) and MNPM (g mol^{-1}) are the total flow gas rates in the reactor and the molar mass of NPM, respectively; t (min) is the irradiation time; C_t^{NOx} (molecules cm^{-3}) is the concentration of gaseous HONO or NOx formed by photolysis of NPM during the irradiation period; N_A is the Avogadro number; M_0 (mg) and M_t (mg) are the masses at the beginning and end of the NPM photolysis experiments.

2.6 Flux densities of HONO and NOx

The flux densities of HONO and NOx were estimated by using the following equations:

$$HONO_{flux} = \frac{[HONO]\cdot V}{s\cdot t} \quad (5)$$

$$NOx_{flux} = \frac{[NOx]\cdot V}{s\cdot t} \quad (6)$$

where HONO flux is expressed in molecules cm^{-2} s^{-1}, [HONO] is the concentration of HONO in molecules cm^{-3}, V (cm^3) is the volume of the reactor, S (cm^2) is the surface of the reactor, and t (s) is the residence time of HONO in the circular reactor.

2.7 Global simulation of NOx and HONO fluxes

We estimated the global inventory of the NOx and HONO fluxes produced by NPM photochemistry using the observation-constrained parametrization scheme and hourly solar radiation data. Gridded and hourly downward solar radiation data are obtained from the Modern-Era Retrospective analysis for Research and Application version 2 (MERRA-2) assimilated meteorological fields. We calculated the flux of NOx and HONO for each model grid at a horizontal resolution of 0.5°×0.625° (consistent with MERRA2 radiation dataset) following Eq-S1, Eq-S2 and Eq-S3, but assuming that the environmental NPM concentration is three orders smaller than the experimental conditions of 0.5 mg L^{-1}. The parameterization of HONO and NOx productions from NPM photolysis at Fe^{3+} concentration of 0.025 mg L^{-1} used in our estimation is based on Eq-S1, Eq-S2 and Eq-S3, and more details can be seen in the Text S2.

3 Results and Discussion

3.1 Absorbance of NPM in the presence of Fe^{3+}

Figure S1 shows the absorbance of NPM (0.05 mg ml^{-1}) in the dilute aqueous phase and at different Fe^{3+} concentrations, adjusted by $FeCl_3$ along with the emission spectrum of the solar simulator and the sunlight. The presence of Fe^{3+} at various initial concentrations slightly enhanced the absorbance of NPM, especially at high Fe^{3+} concentration (0.08 mg ml^{-1}), indicating that no Fe^{3+}-NPM complexes were generated (Liu et al., 2020). Indeed, pH is a sensitive parameter that can significantly affect the light-absorbing properties and the degree of photochemical degradation of organic compounds (Cai et al., 2018; Zhou et al., 2019). The interaction between Fe^{3+} and organics as well as possible aggregation of organics at low pH may also influence the light absorption at low wavelengths (Weishaar et al., 2003). The change of Fe^{3+} concentrations may alter the pH of the system, which in turn may affect the protonation/deprotonation degree of NPM, and therefore affects its absorption spectrum (Zhou et al., 2019). The pH value of the NPM solution in the presence of Fe^{3+} varies between 2.4 and 3.4, and under this pH conditions, NPM (pKa=3.1) exists in both, ionic and neutral form (Hậu et al., 2021; Bonmatin et al., 2015).

3.2 Kinetic analysis

Iron ions are ubiquitous in natural waters with concentrations ranging between 10^{-7} and 10^{-4} M, and even higher in contaminated waters (Li et al., 2018; Faust et al., 1990). Previous studies have shown that iron ions play an important role in the photolysis of pesticides and may affect the photodegradation of organic pollutants (Faust et al., 1990; Zhao et al., 2014). The photolysis kinetics of NPM were performed to account the loss of NPM. The photolysis of NPM at different

concentrations of Fe^{3+} obeyed pseudo-first-order kinetics (Figure 1), with half-lives ranging from 135.1 to 223.6 minutes as the Fe^{3+} concentration increased from 0 to 0.8 mg ml^{-1} (Table S1).

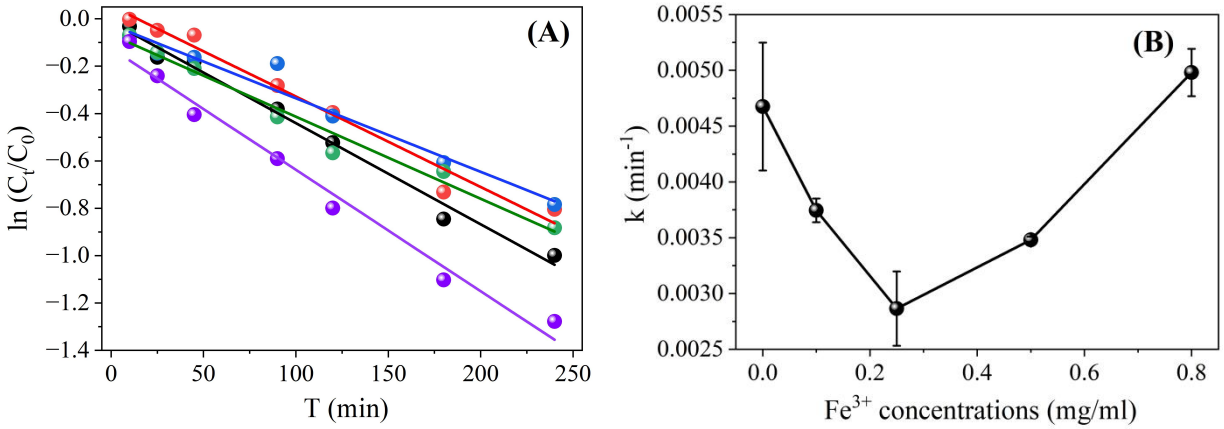

Figure 1. (A) The kinetics of NPM (0.5 mg ml^{-1}) in the absence of Fe^{3+} (dark line), and in the presence of different Fe^{3+} concentrations: 0.1 mg ml^{-1} (red line), 0.25 mg ml^{-1} (blue line), 0.5 mg ml^{-1} (green line) and 0.8 mg ml^{-1} (purple line). (B) The rate constants of NPM light-induced degradation (0.5 mg ml^{-1}) at different Fe^{3+} concentrations.

The light-induced degradation of NPM was significantly inhibited at low Fe^{3+} concentration ($C_{(Fe3+)}$ <0.5 mg ml^{-1}, Figure 1 and Table S1). In contrast, when the concentration of Fe^{3+} reached 0.8 mg ml^{-1}, the degradation of NPM is promoted (Figure 1), exhibiting a rate constant of 0.00513 min^{-1} (Table S1). Previous studies have demonstrated that the degradation of organic compounds in the presence of Fe^{3+} is dose dependent (Lin et al., 2019; Deguillaume et al., 2005). For instance, Fe^{3+} slightly inhibits the photodegradation of fluazaindolizine at concentration of 1-5 mg L^{-1} but promotes its degradation rate at concentrations ranging between 0.1 and 0.5 mg L^{-1} (Lin et al., 2019). Fang et al. (Deguillaume et al., 2005) reported that photodegradation of flupyradifurone, a novel neonicotinoid pesticide, was faster at lower Fe^{3+} concentrations and slowed down with the increase of Fe^{3+} concentration (Deguillaume et al., 2005).

The main reason for the inhibition effect of Fe^{3+} is the attenuation of radiation due to the absorption by Fe^{3+} (light screening), which reduces the light absorbance by NPM and its photodegradation. At the same time, it has been extensively confirmed that $[Fe^{3+}(OH)]^{2+}$ is the main form of Fe^{3+} and exhibits great photoactivity in aqueous solution at pH=3 (Bai et al., 2023; Li et al., 2023). In the presence of $[Fe^{3+}(OH)]^{2+}$, strong oxidizing reactive oxygen species (ROS) are produced, which promote hydroxylation and degradation of NPM (Andrianirinaharivelo et al., 1995; Mazellier et al., 1997). As a result, at pH=3, the photodegradation of NPM is accelerated at high Fe^{3+} concentrations.

In this study, high Fe^{3+} concentration (0.8 mg ml^{-1}) promoted the photodegradation of NPM, and the formation of HONO and NOx (see the section below). The enhanced formation of HONO and NOx can be ascribed to ROS as described in the section 3.5.

3.3 HONO and NOx Formations by NPM Photolysis

The experiments of NPM photodegradation in the aqueous phase were performed to measure the HONO and NOx production in the presence of different Fe^{3+} concentrations. The HONO and NOx production by spontaneous reaction of NPM in dark were negligible (Figure S3). When the NPM samples were exposed to light irradiation the concentrations of HONO and NOx quickly increased (Figure 2A).

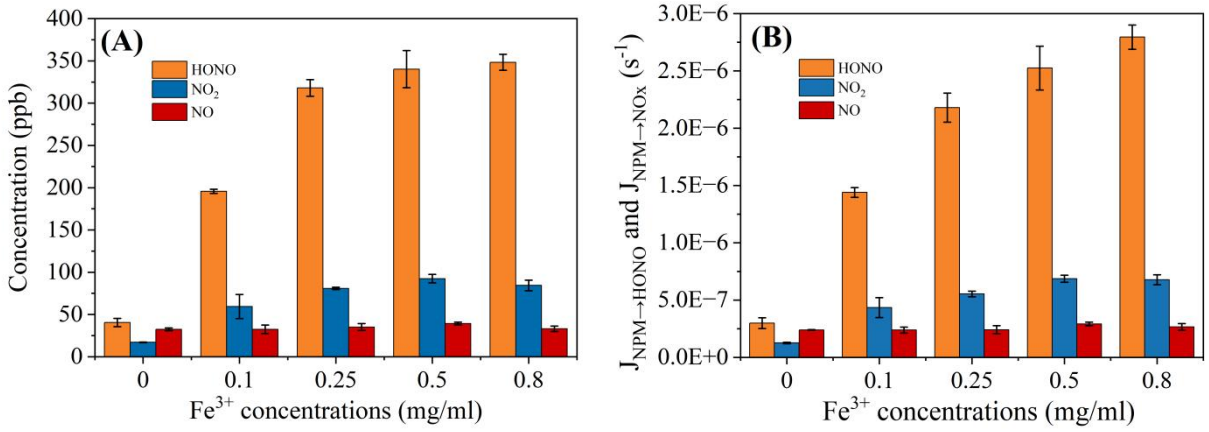

Figure 2. (A) The concentration of NO, NO_2 and HONO produced by NPM photolysis at different concentrations of Fe^{3+}. (B) $J_{NPM\rightarrow HONO}$ and $J_{NPM\rightarrow NOx}$ from NPM at different concentrations of Fe^{3+}. Irradiation intensity of 169.4 W m^{-2} at 300<λ<400 nm, T=298 K.

Only the concentration of NO formed upon irradiation of NPM is almost the same in the absence of Fe^{3+} and in the presence of 0.25 mg mL^{-1} of Fe^{3+} (Figure 2A). In the meantime, the NO_2 formation increased significantly with the increase of Fe^{3+} concentrations and remained almost steady during the whole light exposure time (Figure S3). Moreover, when the experiments were shifted to high concentration of soluble iron (0.25-0.8 mg mL^{-1}), significantly enhanced NO_2 and NO formation were observed, and then slowly decreased with the light exposure time. In order to better understand the effect of iron on HONO and NOx production, the quantities of HONO and NOx were compared when the NPM photolysis reached a relatively stable stage (120 min). It is important to note that, the formed HONO (341 ppb) was significantly higher at the iron concentration of 0.8 mg mL^{-1} compared to the HONO (37 ppb) formed in the absence of iron. Similarly, the quantity of the formed NO_2 increased from 17 ppb in the absence of iron to 96 ppb in the presence of 0.5 mg mL^{-1} of Fe^{3+}. However, further increase of the iron concentration to 0.8 mg mL^{-1} tend to decline the production of NO_2. Figure 2 shows that the NO concentrations almost remained unchanged with the increase of iron concentration. To quantify the photolysis quantum yields of HONO, NO_2 and NO formation from NPM photolysis, we estimated the photolysis frequency of HONO ($J_{NPM\rightarrow HONO}$), NO_2 ($J_{NPM\rightarrow NO2}$) and NO ($J_{NPM\rightarrow NO}$) formation, respectively (Figure 2B). $J_{NPM\rightarrow HONO}$ varied from $(2.99\pm0.46)\times10^{-7}$ s^{-1} in the absence of Fe^{3+} to $(2.79\pm0.10)\times10^{-6}$ s^{-1} in the presence of 0.8 mg ml^{-1} Fe^{3+}. Simultaneously, $J_{NPM\rightarrow NO2}$ increased ca. 5-fold from $(1.25\pm0.06)\times10^{-7}$ s^{-1} in the absence of Fe^{3+} to $(6.77\pm0.44)\times10^{-7}$ s^{-1} at 0.8 mg ml^{-1} Fe^{3+}. Regarding the $J_{NPM\rightarrow NO}$, there was nearly no discernible changes observed, with values ranging from $(2.38\pm0.27)\times10^{-7}$ s^{-1} to $(2.92\pm0.15)\times10^{-7}$ s^{-1}. Previous studies (Yang et al., 2021) have found that the photolysis frequency of HONO and NO in nitrophenol solid-phase films (4-

nitrophenol, 4-nitrocatechol, 3,5-dinitrosalicylic acid, 3-nitrosalicylic acid, and 5-nitrosalicylic acid) varied in the ranges of $(0.34\text{-}4.16) \times 10^{-7}$ and $(0.38\text{-}3.21) \times 10^{-7}$ s^{-1}, respectively, when irradiated by xenon lamps. NPM liquid-phase photolysis produced HONO and NOx at the photolysis frequency of 10^{-7} , but the addition of iron resulted in the photolysis frequency of 10^{-6} for HONO, suggesting that iron significantly facilitated the release of HONO. In order to compare the efficiency of NPM at different Fe^{3+} concentrations in producing HONO and NO, Φ_{HONO} and Φ_{NOx} were displayed (Table S2). It can be concluded that NPM with high Fe^{3+} concentrations had more important HONO formations as compared to pure NPM.

3.4 HONO and NOx Surface Flux Densities

Figure 3 summarizes the results obtained in terms of HONO formation rates per unit of exposed surface area, flux densities of HONO, NO_2, and NO.

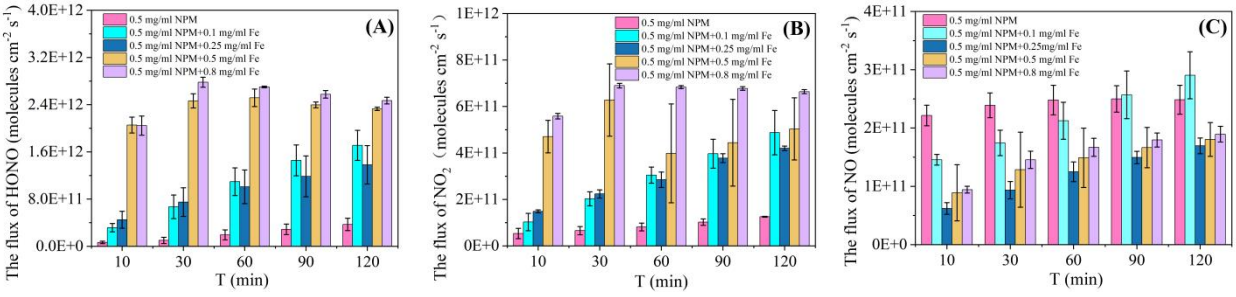

Figure 3. Flux densities of HONO (A), NO_2 (B) and NO (C) determined in function of photolysis time of NPM in the presence of different concentrations of Fe^{3+}.

The flux densities values of HONO and NOx indicate that direct photolysis dominated the transformation process of the NPM samples in the absence of Fe^{3+}. However, the introduction of soluble iron, leads to significantly increased HONO and NO_2 yields during the first 10 min reaction time. The further progress of the reaction up to two hours leads to slightly increased flux densities of NO_2 and HONO. In contrast, the NO formation showed a slow decrease after the addition of Fe^{3+}. A recent study (Aregahegn et al., 2017) demonstrated that photolysis of solid film consisting of imidacloprid (IMD) did not lead to HONO and NOx formation, but N_2O was rather the main gas-phase product. However, it is important to note that the introduction of Fe^{3+} promotes the photodegradation of NPM to produce more HONO and NOx. In the section below we suggest a tentative reaction mechanism to describe the formation of HONO and NO_2 upon irradiation of NPM at the water surface in the presence of soluble iron.

3.5 Mechanism Describing the Formation of HONO and NOx

We speculate that in the presence of Fe^{3+}, the decrease in dissolved nitrogen species that resulted from the photodegradation of NPM is the reason for the formation of HONO and NOx. Therefore, ROS and dissolved nitrogen containing ions were measured upon photodegradation of NPM in the presence of Fe^{3+}. The generation of superoxide radicals (O_2-•), singlet oxygen ($^1O_2$) and hydroxyl radicals (OH) were quantified using DMPO, TEMP and DMPO as chemical probe molecules,

respectively. Figure 4A shows that in the absence of Fe^{3+}, the photodegradation of NPM induces generation of OH, O_2-•, and $^1O_2$, which can be ascribed to the electron transfer between the excited triplet state of NPM and the molecular oxygen (O_2) (Segura et al., 2008; Mostafa et al., 2013; Marin et al., 2012; Wang et al., 2021).

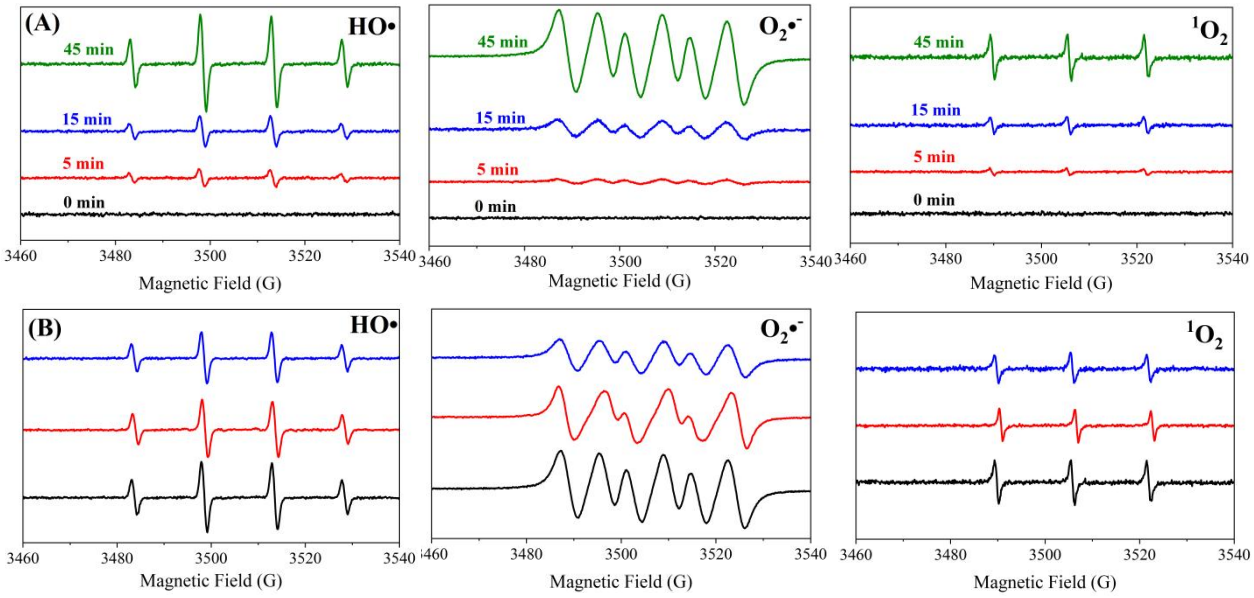

Figure 4. A) EPR spectra obtained upon photodegradation of NPM (0.5 mg ml^{-1}) in the absence of Fe^{3+} as a function of the reaction time. B) EPR spectra obtained upon 45 min photodegradation of NPM (0.5 mg ml^{-1}) in the absence of Fe^{3+} (dark line), and in the presence of 0.25 mg ml^{-1} of Fe^{3+} (red line) and 0.8 mg ml^{-1} of Fe^{3+} (blue line).

It has been reported that under UV light irradiation, Fe^{3+} photo-reduction regenerates Fe^{2+} accelerating the process due to the formation of new OH radicals (Segura et al., 2008). The EPR measurements revealed an interesting phenomenon that the increase of Fe^{3+} concentration promotes the consumption rate of ROS (Figure 4B) rather than the production rate. The generated ROS would react with lower valence nitrogen-containing species to form HONO and NOx. Based on this finding we suggest a tentative reaction mechanism which could explain the formation of large quantities of HONO and NOx during the photochemical degradation of NPM. The photochemical generation of ROS could be driven by two pathways, pathway I: the excited tripled state of NPM (^{3}NPM*) can be formed under light irradiation (R1) (Mora et al., 2021), and then by reacting with water molecules (R2) it can trigger the formation of ROS such as OH radicals, accompanied by the generation of O_2-• through the transformation between radical anion of NPM (NPM-•) and dissolved oxygen (R3) (Wang et al., 2021). Furthermore, with the progress of the photodegradation of NPM, an increase of O_2-• and OH formation was observed (Figure 4A), favoring the HONO and NO_2 formation (R6-R8). In the presence of Fe^{3+}, the formation of OH radicals occur as well by R4 (Mazellier et al., 1997). In addition, nitrate ions (NO_3^-) and nitrite ions (NO_2^-) in the aqueous phase are formed by reactions R5 to R7. Peroxynitrate ($OONO_2^-$) is formed by reaction of O_2-• with NO_2, which thermally decomposes to form NO_2^- and O_2 which further leads to HONO formation (R6) (Wang et al., 2020; Lammel et al., 1990; Goldstein et al., 1998). The reaction between O_2-• and NO can lead to the formation of NO_2^- and NO_3^-, with a relatively fast rate constant of 4.3×10^9

M^{-1} s^{-1} (Goldstein et al., 1995) producing a peroxynitrite ($OONO^-$) which then yields NO_3^- through internal rearrangement (R7) (Løgager et al., 1993). At neutral pH (pKa=6.5), the product OONOH can also be formed by protonation, which can coexist with $OONO^-$ to form NO_2^- (R7) (Guptaet al., 2009). Previous studies have shown that the reaction between OH and NO_2^- will generate NO_2 (R8) (Løgager et al., 1993), and sharp increase of HONO concentration occurs immediately from reaction between NO_2^- and H^+ (R9), which is expected to be an important pathway of HONO formation.

At low Fe^{3+}concentrations (0.25-0.5 mg mL^{-1}), the degradation rate of NPM was completely inhibited which was not the case for higher Fe^{3+} concentration (0.5-0.8 mg mL^{-1}) (Figure 1). Notably, Fe^{3+} plays an important role in providing an acidic environment (pH=2.4-3.4) in the reaction system, which is followed by the redox reaction between Fe^{2+} and NO_3^- to produce NO_2 and consequently increase the amount of NO_2 (R10) (Figure S3). It has been shown that NO_3^- undergo photochemical process and thus produces HONO (R11) and NO_2 (R12) (Ye et al., 2016; Zhou et al.,2011).

$$NPM \xrightarrow{hv} {}^3NPM^* \quad \text{R(1)}$$

$$^3NPM^* + H_2O \rightarrow H^+ + \cdot OH + NPM^{-\cdot} \quad \text{R(2)}$$

$$NPM^{-\cdot} + O_2 \rightarrow NPM + O_2^{-\cdot} \quad \text{R(3)}$$

$$Fe^{3+} + H_2O \xrightarrow{hv} \boldsymbol{Fe^{2+}} + \cdot OH + H^+ \quad \text{R(4)}$$

$$2NO_2 + H_2O \rightarrow HNO_2 + HNO_3 \quad \text{R(5)}$$

$$O_2^{-\cdot} + NO_2 \rightarrow OONO_2^- \rightarrow O_2 + NO_2^- \xrightarrow{+H^+ \ (pKa=3.2)} HONO \quad \text{R(6)}$$

$$O_2^{-\cdot} + NO \rightarrow OONO^- \ (NO_3^-) \leftrightarrows OONOH \xrightarrow{+OONO^-} O_2 + 2NO_2^- + H^+ \xrightarrow{pKa=3.2} \boldsymbol{HONO} \quad \text{R(7)}$$

$$NO_2^- + \cdot OH \rightarrow NO_2 + OH^- \quad \text{R(8)}$$

$$NO_2^- + H^+ \xrightarrow{pKa=3.2} \boldsymbol{HONO} \quad \text{R(9)}$$

$$Fe^{2+} + NO_3^- + 2H^+ \rightarrow Fe^{3+} + NO_2(g) + H_2O \quad \text{R(10)}$$

$$NO_3^- \xrightarrow{hv} [NO_3^-]^* \rightarrow O(^3P) + NO_2^- \xrightarrow{H^+} HONO \quad \text{R(11)}$$

$$NO_3^- \xrightarrow{hv} [NO_3^-]^* \xrightarrow{H^+} NO_2 + \cdot OH \quad \text{R(12)}$$

A simplified illustration of the reaction mechanism is shown in Figure S4. As shown in Figure S3, the HONO and NO_2 production during the photodegradation of NPM in the presence of Fe^{3+} is significantly enhanced relative to that in the absence of iron ions. High Fe^{3+} concentration (0.5-0.8 mg mL^{-1}) promotes the HONO and NO_2 formation compared to low Fe^{3+} concentrations (0.25-0.5 mg mL^{-1}). The formed NO_3^- and NO_2^- were also measured by the ion chromatography analysis to evaluate the effect of Fe^{3+} (see the details in Text S1 and Figure S5). As shown in Figure S5, the concentration of NO_3^-

and NO_2^- decreased sharply in the presence of Fe^{3+} compared to that in absence of Fe^{3+}. These results suggest that HONO and NO_2 enhancement during the irradiation of NPM solutions containing Fe^{3+} can be ascribed to the transformation in the products distribution from NO_3^- and NO_2^- rather than a change in the products formation from the photodegradation of NPM.

4 Conclusions and outlook

Laboratory study revealed the formation of a greenhouse gas N_2O by photolysis of NPM (Aregahegn et al., 2018), but previously the theoretical calculation predicted that the photolysis of NNs can generate NO_2 (Palma et al., 2020).

The current study reveals that the light-induced degradation of NPM leads to enhanced production of HONO and NOx driven by secondary photochemistry between redox reaction of Fe^{3+}/Fe^{2+} and photoproduced ROS. We quantified the photochemical HONO and NOx formation through NPM photodegradation, and we suggest that this chemistry may represent a significant source of HONO and NOx in the regions where surface waters are polluted with NNs insecticides.

In order to estimate the relative importance of the NPM photolysis to global HONO and NOx emissions in the atmosphere, we parametrized the global HONO and NOx production related to NPM photochemistry, based on the NPM photolysis kinetic data and gridded downward solar radiation. The parameterization of HONO and NOx production from NPM photolysis at Fe^{3+} concentration of 0.025 mg L^{-1} used in our estimation is based on Eq-S1, Eq-S2 and Eq-S3. The concentrations of NNs vary from several ng L^{-1} to hundreds of µg L^{-1} (Anderson et al., 2013). In view of the high concentration of NPM (50000 µg L^{-1}) used in our experiments, we selected a rationalization parameter scheme related to the environmental concentration of NPM (50 µg L^{-1}). The kinetic data has shown that the rate constant (k) is faster at low NPM concentration compared to that of high NPM concentrations (Figure S6). Current chemical models do not explicitly consider this source of reactive nitrogen species. In this manner, we are able to generate an hourly dataset of the NOx and HONO fluxes released from NPM chemistry, and we analyze the amount and spatial pattern of the fluxes in Figure 5. We note that although such estimation is rather simplified and can be biased in terms of the spatial heterogeneity as we do not consider the spatial variation of environmental NPM concentrations, our study presents a pioneer attempt to quantify the global source of HONO and NOx from the NPM photochemistry, as current chemical models do not explicitly consider this source of reactive nitrogen species. This inventory can be then applied in chemical models to quantify the environmental impact of HONO and NOx fluxes emerging from NPM photochemistry. The details about parameterization of HONO and NOx production emerged from NPM photochemistry are described in the Text S2. Figure 5 shows the spatial distributions of HONO and NOx fluxes produced from NPM photochemistry in the tested year 2017. The results indicate that globally produced HONO and NOx fluxes based on NPM photochemistry are 0.77 and 0.5 Tg N $year^{-1}$, respectively, making a total of 1.27 Tg N $year^{-1}$.

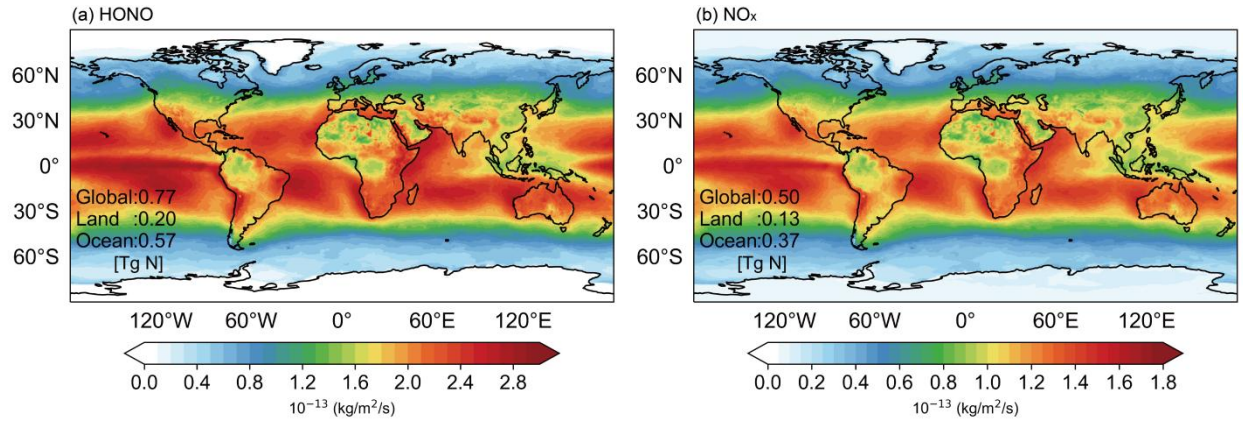

Figure 5. Global emissions of HONO and NOx, produced by photochemistry of NPM in the presence of iron ions for year 2017.

The total production of HONO and NOx emissions due to NPM photochemistry (1.27 Tg N $year^{-1}$) represents 3.5% of the anthropogenic emissions of NOx related to fossil fuel in the year 2017 (36.2 Tg N $year^{-1}$, from the Community Emissions Data System (CEDS) inventory), and about 14.8% of the soil emissions (8.6 Tg N/year (Lu et al., 2021)). The highest HONO and NOx fluxes (74%) are produced by the photochemistry of NPM at the Ocean surface in the presence of iron ions, especially tropical oceans. The latter can be ascribed to the higher solar radiation in the tropic region. As displayed in the Figure S7, it is obvious to see that the spatial distribution of solar radiation is particularly strong in tropical oceanic regions, which can further confirmed the higher HONO and NOx fluxes at the ocean surface. The high reactive nitrogen emissions could also appear over other water surfaces like inland waters and lakes worldwide, through similar mechanisms induced by NPM photochemistry. Further studies are needed to quantify the relative importance of the recognized HONO and NOx sources from NPM photochemistry on a global scale as well as the impact on tropospheric ozone and OH in the marine boundary layer.

Data availability

All raw data can be provided by the corresponding authors upon request.

Author contributions

J.L. and S.G designed the research. Z.R., Y.L. and Y.H. performed the laboratory experiments. J.L., Z.R., X.G., S.L. C.Y., X.L. and S.G. analyzed and interpreted the data from laboratory experiments. Y.H., and Y.L. contributed to the relevant discussion on the manuscript. J.L., Y.H. and S.G. wrote the paper. All authors discussed the results and commented on the manuscript.

Competing interests

The authors declare no competing financial interest.

Acknowledgments

This work was supported by National Natural Science Foundation of China (No. 42207127, 42030712) and Applied Basic Research Foundation of Yunnan Province (Grant No. 202301AT070424, 202101BE070001-027, 202101BG070084). We are grateful to the National Natural Science Foundation of China (42177087 and 41977187), National Natural Science Foundation of China, Research Fund for International Scientists (4221101064), Yunnan Major Scientific and Technological Projects (Grant No. 202302AG050002), Yunnan Revitalization Talents Support Plan Young Talent Project and High-End Foreign Experts Project for financing this research.

Supporting Information

Additional Ten Figures, Three Tables and Supplementary Text. The supporting information is available free of charge via the Internet on the ACS Publications website at http://pubs.acs.org.

References

Alicke, B., Geyer, A., Hofzumahaus, A., Holland, F., Konrad, S., Pätz, H. W., Schäfer, J., Stutz, J., Volz-Thomas, A., and Platt, U.: OH formation by HONO photolysis during the BERLIOZ experiment, J. Geophys. Res. Atmos., 108, doi:10.1029/2001jd000579, 2003.

Anderson, T. A., Salice, C. J., Erickson, R. A., McMurry, S. T., Cox, S. B., and Smith, L. M.: Effects of landuse and precipitation on pesticides and water quality in playa lakes of the southern high plains, Chemosphere., 92, 84-90, doi:10.1016/j.chemosphere.2013.02.054, 2013.

Andrianirinaharivelo, S., Mailhot, G., and Bolte, M.: Photodegradation of organic pollutants induced by complexation with transition metals (Fe3+ and Cu2+) present in natural waters, Sol. Energy Mater. Sol. Cells., 38, 459-474, doi:10.1016/0927-0248(94)00238-x, 1995.

Aregahegn, K. Z., Ezell, M. J., and Finlayson-Pitts, B. J.: Photochemistry of Solid Films of the Neonicotinoid Nitenpyram, Environ. Sci. Technol., 52, 2760-2767, doi:10.1021/acs.est.7b06011, 2018.

Aregahegn, K. Z., Shemesh, D., Gerber, R. B., and Finlayson-Pitts, B. J.: Photochemistry of Thin Solid Films of the Neonicotinoid Imidacloprid on Surfaces, Environ. Sci. Technol., 51, 2660-2668, doi:10.1021/acs.est.6b04842, 2017.

Bai, X., Yang, Q., Guo, Y., Hao, B., Zhang, R., Duan, R., and Li, J.: Alkyl halide formation from degradation of carboxylic acids in the presence of Fe(III) and halides under light irradiation, Water. Res., 235, doi:10.1016/j.watres.2023.119842, 2023.

Bass, C., Denholm, I., Williamson, M. S., and Nauen, R.: The global status of insect resistance to neonicotinoid insecticides, Pestic. Biochem. Physiol., 121, 78-87, doi:10.1016/j.pestbp.2015.04.004, 2015.

Bejan, I., Abd El Aal, Y., Barnes, I., Benter, T., Bohn, B., Wiesen, P., and Kleffmann, J. r.: The photolysis of ortho-nitrophenols: a new gas phase source of HONO, Phys. Chem. Chem. Phys., 8, doi:10.1039/b516590c, 2006.

Bonmatin, J. M., Giorio, C., Girolami, V., Goulson, D., Kreutzweiser, D. P., Krupke, C., Liess, M., Long, E., Marzaro, M., Mitchell, E. A. D., Noome, D. A., Simon-Delso, N., and Tapparo, A.: Environmental fate and exposure; neonicotinoids and fipronil, Environ. Sci. Pollut. Res., 22, 35-67, doi:10.1007/s11356-014-3332-7, 2014.

Botías, C., David, A., Horwood, J., Abdul-Sada, A., Nicholls, E., Hill, E., and Goulson, D.: Neonicotinoid Residues in Wildflowers, a Potential Route of Chronic Exposure for Bees, Environ. Sci. Technol., 49, 12731-12740, doi:10.1021/acs.est.5b03459, 2015.

Brigante, M., Cazoir, D., D'Anna, B., George, C., and Donaldson, D. J.: Photoenhanced Uptake of NO2 by Pyrene Solid Films, J. Phys. Chem. A., 112, 9503-9508, doi:10.1021/jp802324g, 2008.

Cai, J., Zhi, G., Yu, Z., Nie, P., Gligorovski, S., Zhang, Y., Zhu, L., Guo, X., Li, P., He, T., He, Y., Sun, J., and Zhang, Y.: Spectral changes induced by pH variation of aqueous extracts derived from biomass burning aerosols: Under dark and in presence of simulated sunlight irradiation, Atmos. Environ., 185, 1-6, doi:10.1016/j.atmosenv.2018.04.037, 2018.

Cazoir, D., Brigante, M., Ammar, R., D'Anna, B., and George, C.: Heterogeneous photochemistry of gaseous NO2 on solid fluoranthene films: A source of gaseous nitrous acid (HONO) in the urban environment, J. Photochem. Photobiol. A., 273, 23-28, doi:10.1016/j.jphotochem.2013.07.016, 2014.

Cimino, A. M., Boyles, A. L., Thayer, K. A., and Perry, M. J.: Effects of Neonicotinoid Pesticide Exposure on Human Health: A Systematic Review, Environ. Health Perspect., 125, 155-162, doi:10.1289/ehp515, 2017.

Deguillaume, L., Leriche, M., Desboeufs, K., Mailhot, G., George, C., and Chaumerliac, N.: Transition Metals in Atmospheric Liquid Phases: Sources, Reactivity, and Sensitive Parameters, Chem. Rev., 105, 3388-3431, doi:10.1021/cr040649c, 2005.

Ezell, M. J., Wang, W., Shemesh, D., Ni, A., Gerber, R. B., and Finlayson-Pitts, B. J.: Experimental and Theoretical Studies of the Environmental Sensitivity of the Absorption Spectra and Photochemistry of Nitenpyram and Analogs, ACS Earth Space Chem., 3, 2063-2075, doi:10.1021/acsearthspacechem.9b00179, 2019.

Faust, B. C.,and Hoigné, J.: Photolysis of Fe (III)-hydroxy complexes as sources of OH radicals in clouds, fog and rain, Atmos. Environ., Part A., 24, 79-89, doi:10.1016/0960-1686(90)90443-q, 1990.

Fukuhara, K., Kurihara, M., and Miyata, N.: Photochemical Generation of Nitric Oxide from 6-Nitrobenzo[a]pyrene, J. Am. Chem. Soc., 123, 8662-8666, doi:10.1021/ja0109038, 2001.

Gen, M., Zhang, R., and Chan, C. K.: Nitrite/Nitrous Acid Generation from the Reaction of Nitrate and Fe(II) Promoted by Photolysis of Iron–Organic Complexes, Environ. Sci. Technol, 55, 15715-15723, doi:10.1021/acs.est.1c05641, 2021.

Gibbons, D., Morrissey, C., and Mineau, P.: A review of the direct and indirect effects of neonicotinoids and fipronil on vertebrate wildlife, Environ. Sci. Pollut. Res., 22, 103-118, doi:10.1007/s11356-014-3180-5, 2015.

Goldstein, S.,and Czapski, G.: The reaction of NO· with O2·− and HO2·−: A pulse radiolysis study, Free Radical Biol. Med., 19, 505-510, doi:10.1016/0891-5849(95)00034-u, 1995.

Goldstein, S., Czapski, G., Lind, J., and Merenyi, G.: Mechanism of Decomposition of Peroxynitric Ion (O2NOO-): Evidence for the Formation of O2•- and •NO2 Radicals, Inorganic chemistry., 37, 3943-3947, doi:10.1021/ic980051l, 1998.

González-Mariño, I., Rodríguez, I., Rojo, L., and Cela, R.: Photodegradation of nitenpyram under UV and solar radiation: Kinetics, transformation products identification and toxicity prediction, Sci. Total Environ., 644, 995-1005, doi:10.1016/j.scitotenv.2018.06.318, 2018.

Goulson, D., Nicholls, E., Botías, C., and Rotheray, E. L.: Bee declines driven by combined stress from parasites, pesticides, and lack of flowers, Science., 347, doi:10.1126/science.1255957, 2015.

Gupta, D., Harish, B., Kissner, R., and Koppenol, W. H.: Peroxynitrate is formed rapidly during decomposition of peroxynitrite at neutral pH, Dalton Trans., doi:10.1039/b905535e, 2009.

Hallmann, C. A., Foppen, R. P. B., van Turnhout, C. A. M., de Kroon, H., and Jongejans, E.: Declines in insectivorous birds are associated with high neonicotinoid concentrations, Nature., 511, 341-343, doi:10.1038/nature13531, 2014.

Han, C., Yang, W., Wu, Q., Yang, H., and Xue, X.: Heterogeneous Photochemical Conversion of NO2 to HONO on the Humic Acid Surface under Simulated Sunlight, Environ. Sci. Technol., 50, 5017-5023, doi:10.1021/acs.est.5b05101, 2016.

Han, W., Tian, Y., and Shen, X.: Human exposure to neonicotinoid insecticides and the evaluation of their potential toxicity: An overview, Chemosphere., 192, 59-65, doi:10.1016/j. 2017.

Hậu, N. C., Đào, Đ. T. H., and Đào, L. T. A.: Simultaneous Determination of Neonicotinoid Pesticides in Tea-Tree Plantation Soil by Ultra-Performance Liquid Chromatography Tandem Mass Spectrometry. Tạp chí Khoa học., 18, 403-413, https://journal.hcmue.edu.vn/, 2021.

Hayat, W., Zhang, Y. Q., Hussain, I., Du, X. D., Du, M. M., Yao, C. H., Huang, S. B., and Si, F.: Efficient degradation of imidacloprid in water through iron activated sodium persulfate, Chem. Eng. J., 370, 1169-1180, doi:10.1016/j.cej.2019.03.261, 2019.

Kebede, M. A., Bish, D. L., Losovyj, Y., Engelhard, M. H., and Raff, J. D.: The Role of Iron-Bearing Minerals in NO2 to HONO Conversion on Soil Surfaces, Environ. Sci. Technol., 50, 8649-8660, doi:10.1021/acs.est.6b01915, 2016.

Kessler, S. C., Tiedeken, E. J., Simcock, K. L., Derveau, S., Mitchell, J., Softley, S., Radcliffe, A., Stout, J. C., and Wright, G. A.: Bees prefer foods containing neonicotinoid pesticides, Nature., 521, 74-76, doi:10.1038/nature14414, 2015.

Lammel, G., Perner, D., and Warneck, P.: Decomposition of pernitric acid in aqueous solution, J. Phys. Chem., 94, 6141-6144, doi:10.1021/j100378a091, 2002.

Lacson, C. F. Z., de Luna, M. D. G., Dong, C. D., Garcia-Segura, S., and Lu, M. C.: Fluidized-bed Fenton treatment of imidacloprid: Optimization and degradation pathway, Sustainable Environ. Res., 28, 309-314, doi:10.1016/j.serj.2018.09.001, 2018.

Li, C., Zhang, D., Peng, J., and Li, X.: The effect of pH, nitrate, iron (III) and bicarbonate on photodegradation of oxytetracycline in aqueous solution, J. Photochem. Photobiol., A., 356, 239-247, doi:10.1016/j.jphotochem.2018.01.004, 2018.

Li, P., Gemayel, R., Li, X., Liu, J., Tang, M., Wang, X., Yang, Y., Al-Abadleh, H. A., and Gligorovski, S.: Formation of nitrogen-containing gas phase products from the heterogeneous (photo)reaction of NO2 with gallic acid, Commun. Chem., 6, doi:10.1038/s42004-023-01003-3, 2023.

Lin, H., Pang, K., Ma, Y., and Hu, J.: Photodegradation of fluazaindolizine in water under simulated sunlight irradiation: Identification of transformation products and elucidation of transformation mechanism, Chemosphere., 214, 543-552, doi:10.1016/j.chemosphere.2018.09.151, 2019.

Liu, H., Zhang, Z., Tu, Y.-n., Li, Y., Lei, Y., and Tian, S.: Dual roles of Cu2+ complexation with dissolved organic matter on the photodegradation of trace organic pollutants: Triplet- and OH-induced reactions, Sci. Total Environ., 815, doi:10.1016/j.scitotenv.2022.152934, 2022.

Liu, J., Deng, H., Li, S., Jiang, H., Mekic, M., Zhou, W., Wang, Y., Loisel, G., Wang, X., and Gligorovski, S.: Light-Enhanced Heterogeneous Conversion of NO2 to HONO on Solid Films Consisting of Fluorene and Fluorene/Na2SO4: An Impact on Urban and Indoor Atmosphere, Environ. Sci. Technol., 54, 11079-11086, doi:10.1021/acs.est.0c02627, 2020.

Liu, J., Li, B., Deng, H., Yang, Y., Song, W., Wang, X., Luo, Y., Francisco, J. S., Li, L., and Gligorovski, S.: Resolving the Formation Mechanism of HONO via Ammonia-Promoted Photosensitized Conversion of Monomeric NO2 on Urban Glass Surfaces, J. Am. Chem. Soc., doi:10.1021/jacs.3c02067, 2023.

Liu, J., Li, S., Mekic, M., Jiang, H., Zhou, W., Loisel, G., Song, W., Wang, X., and Gligorovski, S.: Photoenhanced Uptake of NO2 and HONO Formation on Real Urban Grime, Environ. Sci. Technol. Lett., 6, 413-417, doi:10.1021/acs.estlett.9b00308, 2019.

Loegager, T., and Sehested, K.: Formation and decay of peroxynitric acid: a pulse radiolysis study, Phys. Chem., 97, 10047-10052, doi:10.1021/j100141a025, 1993.

Lu, X., Ye, X., Zhou, M., Zhao, Y., Weng, H., Kong, H., Li, K., Gao, M., Zheng, B., Lin, J., Zhou, F., Zhang, Q., Wu, D., Zhang, L., and Zhang, Y.: The underappreciated role of agricultural soil nitrogen oxide emissions in ozone pollution regulation in North China, Nat. Commun., 12, doi:10.1038/s41467-021-25147-9, 2021.

Lu, Z., Challis, J. K., and Wong, C. S.: Quantum Yields for Direct Photolysis of Neonicotinoid Insecticides in Water: Implications for Exposure to Nontarget Aquatic Organisms, Environ. Sci. Technol. Lett., 2, 188-192, doi:10.1021/acs.estlett.5b00136, 2015.

Malato, S., Caceres, J., Agüera, A., Mezcua, M., Hernando, D., Vial, J., and Fernández-Alba, A. R.: Degradation of imidacloprid in water by photo-fenton and TiO2 photocatalysis at a solar pilot plant:: A comparative study, Environ. Sci. Technol., 35, 4359-4366, doi:10.1021/es000289k, 2001.

Marin, M. L., Santos-Juanes, L., Arques, A., Amat, A. M., and Miranda, M. A.: Organic Photocatalysts for the Oxidation of Pollutants and Model Compounds, Chem Rev., 112, 1710-1750, doi:10.1021/cr2000543, 2012.

Mazellier, P., Jirkovsky, J., and Bolte, M.: Degradation of Diuron Photoinduced by Iron(III) in Aqueous Solution, Pestic. Sci., 49, 259-267, doi:10.1002/(sici)1096-9063(199703)49:3<259::Aid-ps526>3.0.Co;2-h, 1997.

Millot, F., Decors, A., Mastain, O., Quintaine, T., Berny, P., Vey, D., Lasseur, R., and Bro, E.: Field evidence of bird poisonings by imidacloprid-treated seeds: a review of incidents reported by the French SAGIR network from 1995 to 2014, Environ. Sci. Pollut. Res., 24, 5469-5485, doi:10.1007/s11356-016-8272-y, 2017.

Monge, M. E., D'Anna, B., Mazri, L., Giroir-Fendler, A., Ammann, M., Donaldson, D. J., and George, C.: Light changes the atmospheric reactivity of soot, Proc. Natl. Acad. Sci. U. S. A., 107, 6605-6609, doi:10.1073/pnas.0908341107, 2010.

Mora Garcia, S. L., Pandit, S., Navea, J. G., and Grassian, V. H.: Nitrous Acid (HONO) Formation from the Irradiation of Aqueous Nitrate Solutions in the Presence of Marine Chromophoric Dissolved Organic Matter: Comparison to Other Organic Photosensitizers, ACS Earth Space Chem., 5, 3056-3064, doi:10.1021/acsearthspacechem.1c00292, 2021.

Morrissey, C. A., Mineau, P., Devries, J. H., Sanchez-Bayo, F., Liess, M., Cavallaro, M. C., and Liber, K.: Neonicotinoid contamination of global surface waters and associated risk to aquatic invertebrates: A review, Environ. Int., 74, 291-303, doi:10.1016/j.envint.2014.10.024, 2015.

Mostafa, S., and Rosario-Ortiz, F. L.: Singlet Oxygen Formation from Wastewater Organic Matter, Environ. Sci. Technol., 47, 8179-8186, doi:10.1021/es401814s, 2013.

Nguyen, D. D. D., Huynh, K. A., Nguyen, X. H., and Nguyen, T. P.: Imidacloprid degradation by electro-Fenton process using composite Fe3O4 – Mn3O4 nanoparticle catalyst, Res. Chem. Intermed., 46, 4823-4840, doi:10.1007/s11164-020-04246-0, 2020.

Pan, X., Wang, Z., Chen, C., Li, H., Li, X., Zhang, Q., Wang, X., and Zhang, Y.: Research on the distribution of neonicotinoid and fipronil pollution in the Yangtze River by high-performance liquid chromatography, Anal. Methods., 12, 5581-5590, doi:10.1039/d0ay01558j, 2020.

Raine, N. E., and Gill, R. J.: Tasteless pesticides affect bees in the field, Nature., 521, 38-39, doi:10.1038/nature14391, 2015.

Segura, C., Zaror, C., Mansilla, H. D.and Mondaca, M. A.: Imidacloprid oxidation by photo-Fenton reaction, J. Hazard. Mater., 150, 679-686, doi:10.1016/j.jhazmat.2007.05.018, 2008.

Rózsa, G., Náfrádi, M., Alapi, T., Schrantz, K., Szabó, L., Wojnárovits, L., Takács, E., and Tungler, A.: Photocatalytic, photolytic and radiolytic elimination of imidacloprid from aqueous solution: Reaction mechanism, efficiency and economic considerations, Appl. Catal., B., 250, 429-439, doi:10.1016/j.apcatb.2019.01.065, 2019.

Palma, D., Arbid, Y., Sleiman, M., de Sainte-Claire, P., and Richard, C.: New Route to Toxic Nitro and Nitroso Products upon Irradiation of Micropollutant Mixtures Containing Imidacloprid: Role of NOx and Effect of Natural Organic Matter, Environ. Sci. Technol., 54, 3325-3333, doi:10.1021/acs.est.9b07304, 2020.

Sedaghat, M., Vahid, B., Aber, S., Rasoulifard, M. H., Khataee, A., and Daneshvar, N.: Electrochemical and photo-assisted electrochemical treatment of the pesticide imidacloprid in aqueous solution by the Fenton process: effect of operational parameters, Res. Chem. Intermed., 42, 855-868, doi:10.1007/s11164-015-2059-5, 2016.

Sun, Y. H., and Liu, X.: Efficient visible-light photocatalytic degradation of imidacloprid and acetamiprid using a modified carbon nitride/tungstophosphoric acid composite induced by a nucleophilic addition reaction, Appl. Surf. Sci., 485, 423-431, doi:10.1016/j.apsusc.2019.04.203, 2019.

Soltani-nezhad, F., Saljooqi, A., Shamspur, T., and Mostafavi, A.: Photocatalytic degradation of imidacloprid using GO/FeO/TiO-NiO under visible radiation: Optimization by response level method, Polyhedron, 165, 188-196, doi:10.1016/j.poly.2019.02.012, 2019.

Simon-Delso, N., Amaral-Rogers, V., Belzunces, L. P., Bonmatin, J. M., Chagnon, M., Downs, C., Furlan, L., Gibbons, D. W., Giorio, C., Girolami, V., Goulson, D., Kreutzweiser, D. P., Krupke, C. H., Liess, M., Long, E., McField, M., Mineau, P., Mitchell, E. A. D., Morrissey, C. A., Noome, D. A., Pisa, L., Settele, J., Stark, J. D., Tapparo, A., Van Dyck, H., Van Praagh, J., Van der Sluijs, J. P., Whitehorn, P. R., and Wiemers, M.: Systemic insecticides (neonicotinoids and fipronil): trends, uses, mode of action and metabolites, Environ. Sci. Pollut. Res., 22, 5-34, doi:10.1007/s11356-014-3470-y, 2015.

Vione, D., and Scozzaro, A.: Photochemistry of Surface Fresh Waters in the Framework of Climate Change, Environ. Sci. Technol., 53, 7945-7963, doi:10.1021/acs.est.9b00968, 2019.

Wan, D., Sharma, V. K., Liu, L., Zuo, Y. G., and Chen, Y.: Mechanistic Insight into the Effect of Metal Ions on Photogeneration of Reactive Species from Dissolved Organic Matter, Environ. Sci. Technol., 53, 5778-5786, doi:10.1021/acs.est.9b00538, 2019.

Wang, W., Ezell, M. J., Lakey, P. S. J., Aregahegn, K. Z., Shiraiwa, M., and Finlayson-Pitts, B. J.: Unexpected formation of oxygen-free products and nitrous acid from the ozonolysis of the neonicotinoid nitenpyram, Proc. Natl. Acad. Sci., 117, 11321-11327, doi:10.1073/pnas.2002397117, 2020.

Wang, W. C., Huang, D. Y., Wang, D. X., Tan, M. X., Geng, M. Y., Zhu, C. Y., Chen, N., and Zhou, D. M.: Extensive production of hydroxyl radicals during oxygenation of anoxic paddy soils: Implications to imidacloprid degradation, Chemosphere, 286, doi:ARTN 13156510.1016/j.chemosphere.2021.131565, 2022.

Wang, W. H., Aregahegn, K. Z., Andersen, S. T., Ni, A. Z., Rohrbacher, A. F., Nielsen, O. J., and Finlayson-Pitts, B. J.: Quantum Yields and NO2 Formation from Photolysis of Solid Films of Neonicotinoids, J. Agric. Food Chem., 67, 1638-1646, doi:10.1021/acs.jafc.8b05417, 2019.

Wang, X., Dalton, E. Z., Payne, Z. C., Perrier, S., Riva, M., Raff, J. D., and George, C.: Superoxide and Nitrous Acid Production from Nitrate Photolysis Is Enhanced by Dissolved Aliphatic Organic Matter, Environ. Sci. Technol. Lett., 8, 53-58, doi:10.1021/acs.estlett.0c00806, 2020.

Wang, Y., Huang, D. D., Huang, W., Liu, B., Chen, Q., Huang, R., Gen, M., Mabato, B. R. G., Chan, C. K., Li, X., Hao, T., Tan, Y., Hoi, K. I., Mok, K. M., and Li, Y. J.: Enhanced Nitrite Production from the Aqueous Photolysis of Nitrate in the Presence of Vanillic Acid and Implications for the Roles of Light-Absorbing Organics, Environ. Sci. Technol., 55, 15694-15704, doi:10.1021/acs.est.1c04642, 2021.

Weishaar, J. L., Aiken, G. R., Bergamaschi, B. A., Fram, M. S., Fujii, R., and Mopper, K.: Evaluation of Specific Ultraviolet Absorbance as an Indicator of the Chemical Composition and Reactivity of Dissolved Organic Carbon, Environ. Sci. Technol., 37, 4702-4708, doi:10.1021/es030360x, 2003.

Yang, W., You, D., Li, C., Han, C., Tang, N., Yang, H., and Xue, X.: Photolysis of Nitroaromatic Compounds under Sunlight: A Possible Daytime Photochemical Source of Nitrous Acid?, Environ. Sci. Technol. Lett., 8, 747-752, doi:10.1021/acs.estlett.1c00614, 2021.

Ye, C., Gao, H., Zhang, N., and Zhou, X.: Photolysis of Nitric Acid and Nitrate on Natural and Artificial Surfaces, Environ. Sci. Technol., 50, 3530-3536, doi:10.1021/acs.est.5b05032, 2016.

Ye, C., Zhang, N., Gao, H., and Zhou, X.: Photolysis of Particulate Nitrate as a Source of HONO and NOx, Environ. Sci. Technol., 51, 6849-6856, doi:10.1021/acs.est.7b00387, 2017.

Young, C. J., Washenfelder, R. A., Roberts, J. M., Mielke, L. H., Osthoff, H. D., Tsai, C., Pikelnaya, O., Stutz, J., Veres, P. R., Cochran, A. K., VandenBoer, T. C., Flynn, J., Grossberg, N., Haman, C. L., Lefer, B., Stark, H., Graus, M., de Gouw, J., Gilman, J. B., Kuster, W. C., and Brown, S. S.: Vertically Resolved Measurements of Nighttime Radical Reservoirs in Los Angeles and Their Contribution to the Urban Radical Budget, Environ. Sci. Technol., 46, 10965-10973, doi:10.1021/es302206a, 2012.

Zhao, Q., Zhao, H., Quan, X., Chen, S., and Zhang, Y.: Photochemical transformation of 2,2′,4,4′-tetrabromodiphenyl ether (BDE-47) in surface coastal waters: Effects of chloride and ferric ions, Mar. Pollut. Bull., 86, 76-83, doi:10.1016/j.marpolbul.2014.07.040, 2014.

Zheng, J., Shi, X., Ma, Y., Ren, X., Jabbour, H., Diao, Y., Wang, W., Ge, Y., Zhang, Y., and Zhu, W.: Contribution of nitrous acid to the atmospheric oxidation capacity in an industrial zone in the Yangtze River Delta region of China, Atmos. Chem. Phys., 20, 5457-5475, doi:10.5194/acp-20-5457-2020, 2020.

Zhou, S., Young, C. J., VandenBoer, T. C., Kowal, S. F., and Kahan, T. F.: Time-Resolved Measurements of Nitric Oxide, Nitrogen Dioxide, and Nitrous Acid in an Occupied New York Home, Environ. Sci. Technol., 52, 8355-8364, doi:10.1021/acs.est.8b01792, 2018.

Zhou, W., Mekic, M., Liu, J., Loisel, G., Jin, B., Vione, D., and Gligorovski, S.: Ionic strength effects on the photochemical degradation of acetosyringone in atmospheric deliquescent aerosol particles, Atmos. Environ., 198, 83-88, doi:10.1016/j.atmosenv.2018.10.047, 2019.

Zhou, X., Zhang, N., TerAvest, M., Tang, D., Hou, J., Bertman, S., Alaghmand, M., Shepson, P. B., Carroll, M. A., Griffith, S., Dusanter, S., and Stevens, P. S.: Nitric acid photolysis on forest canopy surface as a source for tropospheric nitrous acid, Nat. Geosci., 4, 440-443, doi:10.1038/ngeo1164, 2011.